Navier-Stokes Computations of Lee-Side Flows over Delta Wings

James L. Thomas*
NASA Langley Research Center, Hampton, Virginia
and
Richard W. Newsome†
Air Force Wright Aeronautical Laboratories, Wright-Patterson Air Force Base, Ohio

Solutions to the Navier-Stokes equations for the flow over delta wings, with emphasis on the separated vortical flows developing on the lee side at high angles of attack, are obtained. The computations are made with a recently developed implicit algorithm, employing upwind differencing for the pressure and convection terms and central differencing for the shear stress and heat-transfer terms. Solutions to both the three-dimensional equations and the approximate conical-flow equations are compared parametrically with a recently obtained, extensive experimental data base, including variations in leading-edge sweep angle, angle of attack, and Mach number. The computations indicate that the conical-flow approximation provides results in close agreement with the three-dimensional equations, even to angles of attack as high as 20 deg. Good agreement with experimentally measured pressures and vapor-screen photographs, including separated vortical flow over a delta wing and the transition to other flow patterns as the sweep angle and Mach number are varied, is obtained for the matrix of test conditions investigated.

Nomenclature

c = speed of sound
C_n = upper-surface normal-force coefficient
C_p = pressure coefficient
e = total energy per unit volume
F,G,H = inviscid fluxes
H_v = viscous flux
J = transformation Jacobian
L = reference length, taken as root chord
M = Mach number
p = static pressure, $p = (\gamma - 1)[e - \rho(u^2 + v^2 + w^2)/2]$
Pr = Prandtl number, taken as 0.72
$\dot{q}_{x_i}$ = heat flux terms
Q = conservation variables
Re_L = Reynolds number, $Re_L = \tilde{\rho}_\infty \tilde{u}_\infty \tilde{L}/\tilde{\mu}_\infty$
t = time
u,v,w = Cartesian velocities in x, y, and z directions
U,V,W = contravariant velocities
x,y,z = Cartesian coordinates
α = angle of attack
γ = ratio of specific heats, taken as 1.4
δ,Δ = difference operators
Δt = time step
ΔQ = change in Q over time step Δt
λ = coefficient of bulk viscosity, $\lambda + 2\mu/3 = 0$
Λ = sweep angle
μ = coefficient of molecular viscosity
ξ,η,ζ = general curvilinear coordinates
ρ = density
$\tau_{x_i x_j}$ = viscous shear stress terms

Subscripts

LE = leading edge
N = normal to leading edge
x,y,z = differentiation with respect to x,y,z
u = upper-surface value
∞ = conditions at freestream

Superscripts

$\hat{}$ = quantities in generalized coordinates
$\tilde{}$ = dimensional value
$\pm$ = forward and backward contributions

Introduction

THE current interest in high angle-of-attack aerodynamics and vortical flows has focused considerable attention on the experimental and numerical simulation of the flow about a swept delta wing at moderate to high angles of attack. Stanbrook and Squire[1] demonstrated that the change from attached to leading-edge separated flow could be correlated in terms of the Mach number and angle of attack normal to the leading edge. Recent experimental results of Miller and Wood[2] for a series of sharp-edged delta wings are shown in the left portion of Fig. 1. For subsonic leading edges, the flow separates at the leading edge and forms the classical vortex separation, characterized by two counter-rotating vortices on opposite sides of the leeward wing surface. The vortices induce a suction pressure on the upper surface that results in an additional lift component not predicted by linear theory. The transition to other flow patterns as classified by Miller and Wood[2] is shown; in general, as the Mach number is increased or angle of attack decreased, the vortices become flatter and eventually give way to attached flow. Although much progress has been made in the development of approximate methods for such flows, interest here is restricted to methods that solve the Navier-Stokes equations. The Navier-Stokes equations model all physical mechanisms and, as such, set the standard by which less exact solutions may be judged. Vigneron et al.[3] solved the conical and parabolic approximations to the Navier-Stokes equations for the vortical flow about a sharp-edged delta wing at supersonic speeds. Rizzetta et al.[4,5] presented three-dimensional Navier-Stokes solutions for the same sharp-edged delta wing at supersonic and hypersonic speeds. Fujii and Kutler[6,7] solved the three-dimensional Navier-Stokes equations for the leading-edge separation about a delta wing with rounded edges at subsonic speeds. The principal drawbacks of the Navier-Stokes equations are the high computational costs necessary to resolve small-scale

Received June 3, 1986; revision received Sept. 25, 1988.

*Senior Research Scientist, Analytical Methods Branch, Fluid Dynamics. Associate Fellow AIAA.

†Major, U.S. Air Force; currently assigned to U.S. Space Command, Cheyenne, MT AFS Company. Member AIAA.

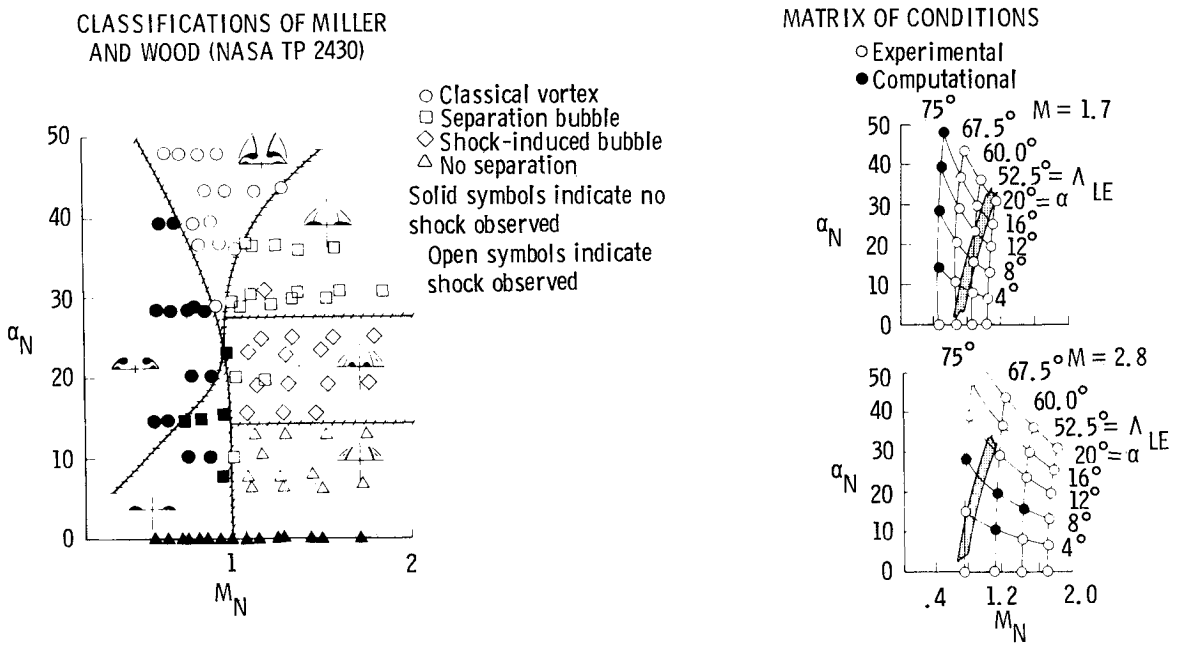

Fig. 1 Classification of experimental data for sharp-edged delta wings from Miller and Wood[2] (left) and matrix of experimental and computational test conditions at $M = 1.7$ and $M = 2.8$ (right).

viscous effects and the need to model turbulence in an approximate manner.

If interest is restricted to supersonic flow past conical bodies, then the governing equations can be simplified by assuming that the resultant flow also will be conical. A conical flow has the property that all flow quantities are invariant on rays that pass through the apex of the conical surface. All derivatives in the radial direction then may be neglected, reducing a three-dimensional problem into a much more tractable two-dimensional one. The conical assumption is exact for inviscid flow. For viscous flow, a length-scale dependence is contained in the Reynolds number; the flow may be thought of as locally conical with the Reynolds number determining the location of the conical plane at which the solution is determined. McRae[8] and McRae and Hussaini[9] computed viscous flows over conical bodies using the conical assumption and showed good agreement with experiment, including the prediction of the vortical flow resulting from separation over a smooth surface at high angles of attack. Solutions to both the conical-flow and three-dimensional equations are obtained in the present paper for the supersonic flow over delta wings at high angles of attack. The numerical solutions are obtained with extensions to a recently developed implicit algorithm,[10,11] employing upwind differencing for the pressure and convective terms and central differencing for the shear stress and heat-transfer terms. The thin-layer form of the governing equations is solved in which only viscous terms normal to the body are retained.

The delta wings considered include the sharp-edged 75-deg swept delta wing studied experimentally by Monnerie and Werlé[12] and computationally by Vigneron et al.[3] and Rizzetta and Shang[4] and Buter and Rizzetta.[5] Computations are also compared with the recent experimental investigations of Miller and Wood,[2] including parametric variations in leading-edge sweep angle and Mach number, at angles of attack up to 20 deg. At several conditions, solutions to the conical-flow equations are compared with solutions to the full three-dimensional equations with a three-dimensional grid.

Governing Equations

The governing equations are the thin-layer approximations to the three-dimensional, time-dependent, compressible Navier-Stokes equations, written in generalized coordinates and conservation form as

$$\frac{\partial \hat{Q}}{\partial t}+\frac{\partial \hat{F}}{\partial \xi}+\frac{\partial \hat{G}}{\partial \eta}+\frac{\partial(\hat{H}-\hat{H}_v)}{\partial \zeta}=0 \tag{1}$$

$$\hat{Q}=\frac{Q}{J}=\frac{1}{J}\begin{bmatrix}\rho\\ \rho u\\ \rho v\\ \rho w\\ e\end{bmatrix}, \quad \hat{F}=\frac{1}{J}\begin{bmatrix}\rho U\\ \rho U u+\xi_x p\\ \rho U v+\xi_y p\\ \rho U w+\xi_z p\\ (e+p)U\end{bmatrix} \tag{2}$$

$$\hat{G}=\frac{1}{J}\begin{bmatrix}\rho V\\ \rho V u+\eta_x p\\ \rho V v+\eta_y p\\ \rho V w+\eta_z p\\ (e+p)V\end{bmatrix}, \quad \hat{H}=\frac{1}{J}\begin{bmatrix}\rho U\\ \rho U u+\xi_x p\\ \rho U v+\xi_y p\\ \rho U w+\xi_z p\\ (e+p)U\end{bmatrix} \tag{3}$$

$$\hat{H}_v=\frac{1}{J}\begin{bmatrix}0\\ \zeta_x\tau_{xx}+\zeta_y\tau_{xy}+\chi_z\tau_{xz}\\ \zeta_x\tau_{yx}+\zeta_y\tau_{yy}+\zeta_z\tau_{yz}\\ \zeta_x\tau_{zx}+\zeta_y\tau_{zy}+\zeta_z\tau_{zz}\\ \zeta_x b_x+\zeta_y b_y+\zeta_z b_z\end{bmatrix} \tag{4}$$

$$U=\xi_x u+\xi_y v+\xi_z w \tag{5a}$$

$$V=\eta_x u+\eta_y v+\eta_z w \tag{5b}$$

$$W=\zeta_x u+\zeta_y v+\zeta_z w \tag{5c}$$

The equations are nondimensionalized in terms of the freestream density and sound speed. The shear stress and heat-flux terms are defined in tensor notation (summation convection implied) as

$$\tau_{x_i x_j} = \frac{M_\infty}{Re_L}\left[\mu\left(\frac{\partial u_i}{\partial x_j}+\frac{\partial u_j}{\partial x_i}\right)+\lambda\frac{\partial u_k}{\partial x_k}\delta_{ij}\right] \tag{6}$$

$$\dot{q}_{x_i} = -\left[\frac{M_\infty \mu}{Re_L Pr(\gamma-1)}\right]\frac{\partial(c^2)}{\partial x_i} \tag{7}$$

$$b_{x_i} = u_j\tau_{x_i x_j} - \dot{q}_{x_i} \tag{8}$$

where the length L is taken as the length from the body apex to the crossflow solution plane for conical flows. The chain rule is used to evaluate derivatives with respect to x,y,z in terms of ξ,η,ζ. Consistent with the thin-layer assumption, only those derivatives in the direction normal to the wall ζ are retained in the shear stress and heat-flux terms. Equation (1) is closed by Stokes' hypothesis for bulk viscosity and Sutherland's law for molecular viscosity. All calculations presented are for laminar flow.

Computational Method

Upwind solutions were obtained with the flux vector-splitting algorithm developed by Thomas et al.[10] and Thomas and Walters.[11] The generalized fluxes $\hat{F},\hat{G},\hat{H}$, representing pressure and convection terms, are split into forward and backward contributions according to the sign of the eigenvalues of the Jacobian matrices

$$\frac{\partial\hat{F}}{\partial Q},\frac{\partial\hat{G}}{\partial Q},\frac{\partial\hat{H}}{\partial Q}$$

and differenced accordingly. For example, the flux difference in the ξ direction is

$$(\delta_\xi\hat{F})_i = (\delta_\xi^-\hat{F}^+ + \delta_\xi^+\hat{F}^-)_i \tag{9}$$

The flux vector in three-dimensional generalized coordinates is split according to the scheme of van Leer.[10] The flux $\hat{F}$, for example, is split according to the streamwise contravariant Mach number, $M_\xi = \bar{u}/c = U/(c|\nabla\xi|)$. For supersonic flow,

$$M_\xi \geq +1 : \hat{F}^+ = \hat{F}, \qquad \hat{F}^- = 0 \tag{10a}$$

$$M_\xi \leq -1 : \hat{F}^- = \hat{F}, \qquad \hat{F}^+ = 0 \tag{10b}$$

and for subsonic flow, $|M_\xi| \leq 1$,

$$\hat{F}^\pm = \frac{|\nabla\xi|}{J}\begin{bmatrix} f^\pm_{\text{mass}} \\ f^\pm_{\text{mass}}[\hat{k}_x(-\bar{u}\pm 2c)/\gamma + u] \\ f^\pm_{\text{mass}}[\hat{k}_y(-\bar{u}\pm 2c)/\gamma + v] \\ f^\pm_{\text{mass}}[\hat{k}_z(-\bar{u}\pm 2c)/\gamma + w] \\ f^\pm_{\text{energy}} \end{bmatrix} \tag{11}$$

where

$$f^\pm_{\text{mass}} = \pm\rho c(M_\xi \pm 1)^2/4$$

$$f^\pm_{\text{energy}} = f^\pm_{\text{mass}}\left[\frac{(1-\gamma)\bar{u}^2 \pm 2(\gamma-1)\bar{u}c + 2c^2}{(\gamma^2-1)} + \frac{(u^2+v^2+w^2)}{2}\right]$$

The equations are written in generalized coordinates but are solved with a finite-volume approach where the metric terms are evaluated geometrically. The surface area of the cell interface in the ξ direction is $|\nabla\xi|$, the cell volume is $1/J$, and

$$(\hat{k}_x,\hat{k}_y,\hat{k}_z) = (\xi_x,\xi_y,\xi_z)/|\nabla\xi|$$

are the direction cosines of the cell interfaces in the ξ direction, corresponding to the choice $\Delta\xi = 1$.

The split-flux differences are implemented as a flux balance across a cell, as

$$(\delta_\xi^-\hat{F}^+ + \delta_\xi^+\hat{F}^-)_i = [\hat{F}^+(Q^-) + \hat{F}^-(Q^+)]_{i+\frac{1}{2}} - [\hat{F}^+(Q^-) + \hat{F}^-(Q^+)]_{i-\frac{1}{2}} \tag{12}$$

The notation $\hat{F}^\pm(Q^\mp)_{i+\frac{1}{2}}$ denotes a split flux evaluated at state variables obtained by second-order upwind-biased interpolations and with the metric terms at the cell interface $(i+\frac{1}{2})$.

Differencing for the diffusion terms representing shear stress and heat-transfer effects corresponds to a second-order accurate central differences in which second derivatives are treated as differences across cell interfaces of first derivative terms, as

$$\delta_\zeta\hat{H}_{v,k} = \hat{H}_{v,k+\frac{1}{2}} - \hat{H}_{v,k-\frac{1}{2}} \tag{13}$$

For example, the term

$$\mu\left(\frac{\partial u}{\partial y}+\frac{\partial v}{\partial x}\right) \tag{14}$$

under the thin-layer approximation becomes

$$\mu\left(\zeta_y\frac{\partial u}{\partial\zeta}+\zeta_x\frac{\partial v}{\partial\zeta}\right) \tag{15}$$

and is differenced in $\hat{H}_{v,k+\frac{1}{2}}$ as

$$\mu_{k+\frac{1}{2}}(\zeta_{y,k+\frac{1}{2}}\delta_\zeta u_{k+\frac{1}{2}} + \zeta_{x,k+\frac{1}{2}}\delta_\zeta v_{k+\frac{1}{2}}) \tag{16}$$

where $\delta_\zeta u_{k+\frac{1}{2}} = u_{k+1} - u_k$.

As described in Ref. 10, the solution is advanced to steady state through streamwise relaxation (ξ direction) and approximate factorization in the crossflow (η,ζ) plane as

$$\left[N + \delta_\eta\frac{\partial\hat{G}}{\partial Q}\right]N^{-1}\left[N + \delta_\zeta\left(\frac{\partial\hat{H}}{\partial Q}-\frac{\partial\hat{H}_v}{\partial Q}\right)\right]\Delta Q^n = R(Q^{n+1},Q^n) \tag{17}$$

where

$$N_i = I/(J\,\Delta t)_i + \left(\frac{\partial\hat{F}^+}{\partial Q}\right)_{i+\frac{1}{2}} - \left(\frac{\partial\hat{F}^-}{\partial Q}\right)_{i-\frac{1}{2}} \tag{18}$$

In general, the solution is obtained by alternate forward and backward sweeping through the crossflow planes with a nonlinear update of the residual R indicated on the right side of Eq. (17). The spatial implicit discretization is taken as first order with no loss in steady-state accuracy; each iteration of Eq. (17) then requires only the solution of two block tridiagonal equations in each crossflow plane.

For the conical-flow solutions, a single array of crossflow volumes is constructed such that the inflow and outflow planes, surfaces of constant ξ, are scaled by the conical transformation

$$y = Yx, \qquad z = Zx$$

where the surface at a unit axial location is defined in terms of the conical variables Y and Z. At each iteration, the inflow conditions are updated with the results of the previous iteration so that at convergence $\partial Q/\partial\xi = 0$, consistent with the conical-flow approximation.[13]

The solutions in all cases were impulsively started from freestream initial conditions. Boundary conditions consist of freestream conditions on the outer boundary, reflection conditions in the crossflow symmetry plane, and no-slip, adiabatic

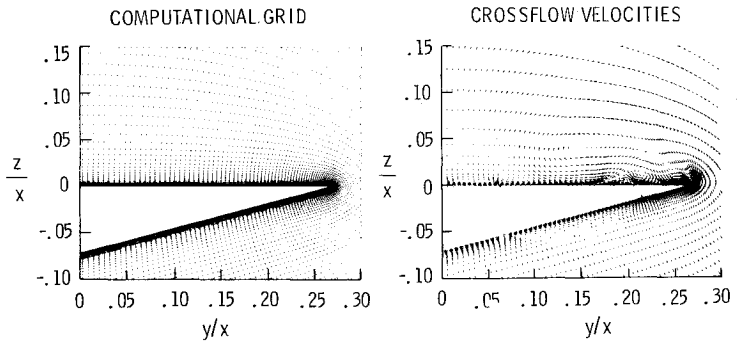

Fig. 2 Computational grid (left) and crossflow velocity vectors (right) for sharp-edged delta wing of Monnerie and Werlé,[12].

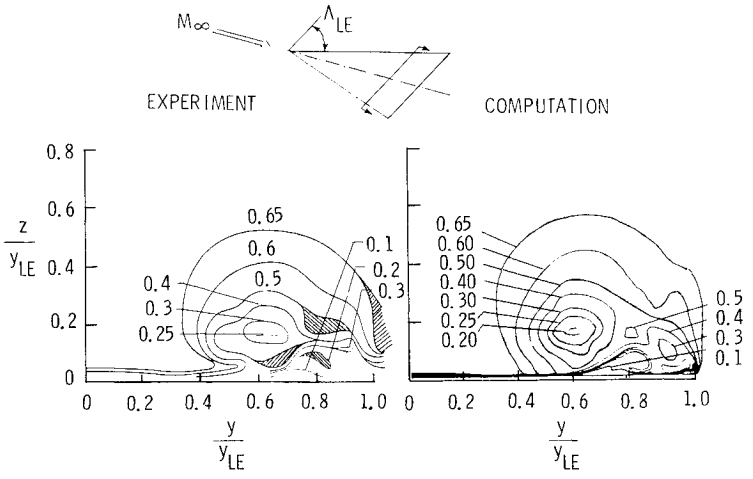

Fig. 3 Experimental (left) and computed (right) pitot pressures for sharp-edged delta wing of Monnerie and Werlé,[12] $M_\infty = 1.95$, $\alpha = 10$ deg, $\Lambda = 75$ deg, $Re_L = 0.95 \times 10^6$.

wall or specified wall temperature conditions on the body surface.

Sharp-Edged Delta Wing Solutions

Comparisons are presented below with the experimental results of Monnerie and Werlé[12] for the flow over a sharp-edged delta wing at $M_\infty = 1.95$ and $Re_L = 0.95 \times 10^6$. The wing tested was swept 75 deg and was flat on the upper surface, of triangular cross section over most of the wing with a maximum thickness of 5%. A conical-flow solution is obtained using the crossflow grid shown in Fig. 2, corresponding to 151 and 75 points circumferential and normal to the surface, respectively, with a minimum normal spacing at the surface of 1×10^{-4}. A comparison of computed and experimental pitot pressures at $x/L = 0.8$ is shown in Fig. 3. The crossflow velocity vectors (Fig. 2) indicate a primary and secondary vortex centered at y/y_{LE} of 55 and 82%, respectively. The computed pitot pressures are based on the Rayleigh pitot tube formula, assuming the probe to be aligned with the local velocity vector and, in general, agree closely with the experimental results. The shaded regions in the experimental data correspond to regions of nearly isobaric pressure. The spanwise positions of the primary and secondary vortices inferred from the pitot pressures agree closely between computation and experiment.

Early on, Vigneron et al.[3] presented parabolic and conical Navier-Stokes solutions for this case. Although relatively coarse grids (36×50) were used, primary and secondary vortices were predicted. The secondary separation predicted was much further outboard than experiment, attributed herein to the coarseness of the computational grid. Rizzetta and Shang[4] computed three-dimensional solutions for this case with a mesh of 70×50 in the crossflow plane. Good comparisons of pitot pressure contours with the experimental and the present results were obtained. Although not shown, the minimum pressure coefficient in the present results (-0.26) is lower than that of either Vigneron et al.[3] (-0.20) or Rizzetta and Shang[4] (-0.23). The differences are attributed to the truncation error associated with the different meshes; the minimum normal spacing at the surface used here is a factor of 10 smaller than that used in Ref. 4. Murman et al.[14] presented Euler solutions for this condition and showed good agreement with pitot pressure in the region of the primary vortex. With the inviscid equations, a crossflow shock is predicted under the primary vortex, which leads to a small shock-induced secondary separation near the leading edge.

Conical-flow computations are compared below with the experimental results of Miller and Wood[2] for a series of sharp-edged delta wings over a range of Mach numbers and angles of attack. The matrix indicating the experimental test conditions and the present computations is shown in the right portion of Fig. 1. Computations are made at $M_\infty = 1.7$ and 2.8; experimental results are also available at $M_\infty = 2.0$ and 2.4. Based upon constant tunnel conditions ($Re/\text{ft} = 2 \times 10^6$) and a uniform wing semispan of 6 in., the Reynolds numbers at the location of the static pressure probes corresponding to leading-edge sweep angles of 75, 67.5, and 60 deg are 3.56, 2.25, and 1.56×10^6, respectively.

The wings tested experimentally were of small thickness ratio, flat on the upper surface, and beveled on the lower surface at the included angle of 10 deg. Since the flow on the lee side is of interest, the computations were made on an

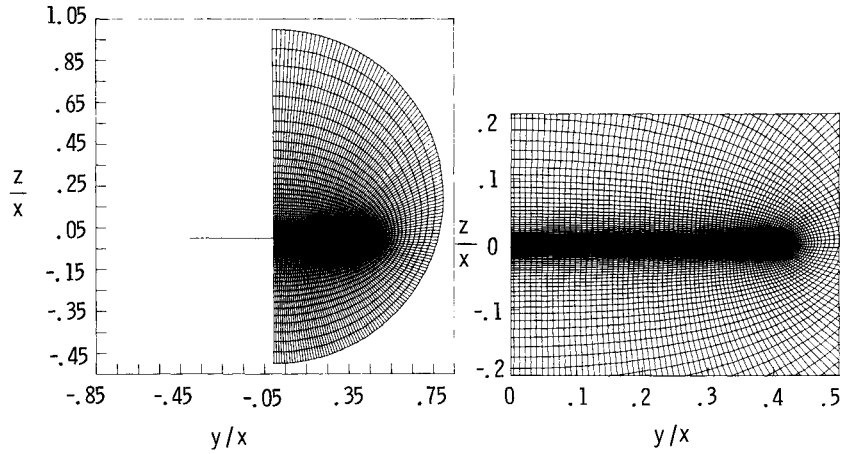

Fig. 4 Typical computational grid for sharp-edged delta wing.

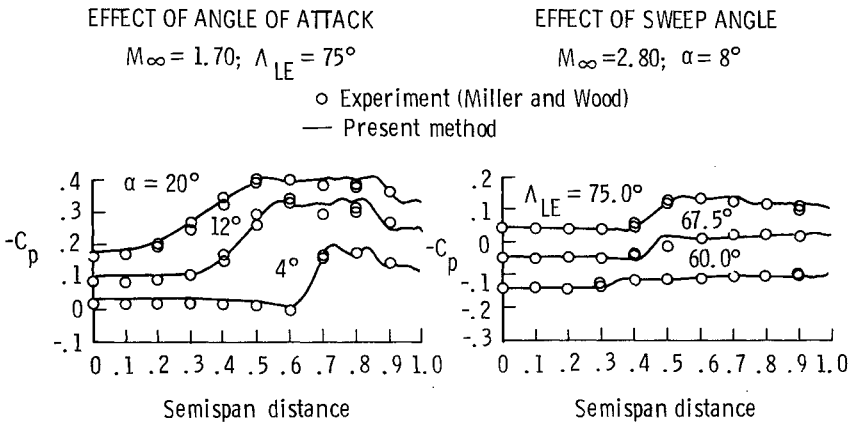

Fig 5. Upper-surface pressure-coefficient distributions.

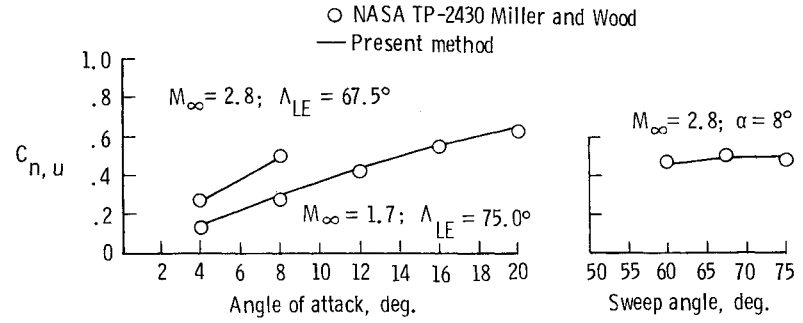

Fig. 6 Upper-surface contributions to normal-force coefficient.

infinitesimally thin wing with a grid generated from a conformal transformation. The grid had dimensions of 151 points circumferentially and 75 points radially, clustered exponentially near the surface. A typical grid is shown in Fig. 4; the minimum grid spacing at the wall is on the order of 1×10^{-5}, and a geometric stretching is used in the outer portion of the grid. The minimum spacing at the wall was varied from 1×10^{-5} to 4×10^{-5} with no effect on the computed pressures. The conical-flow solutions were obtained in 1000 iterations, corresponding to a 4 order of magnitude reduction in the L_2 norm of the residual.

A comparison of computed and experimental pressure coefficients on the upper surface of the 75-deg swept delta wing at a Mach number of 1.7 is shown in Fig. 5 at angles of attack of 4, 12, and 20 deg. The influence of the primary and secondary vortices is evident in the computed pressures, which show overall good agreement with the experimental results. The level of pressure is slightly lower than the experiment in the region of the secondary vortex. The contribution of the upper surface to the normal force coefficient defined as

$$C_{n,u} = -\int_0^1 \frac{2C_p}{\gamma M_\infty^2} \, \mathrm{d}\left(\frac{y}{y_{LE}}\right)$$

is shown in Fig. 6 and indicates close agreement of the computations with experiment, especially at the higher Mach number conditions shown.

The effect of sweep on the upper-surface pressure distribution and normal force coefficient is also shown in Figs. 5 and 6 for a Mach number of 2.8 and an angle of attack of 8 deg. From the flow visualizations of Miller and Wood,[2] it can be seen that as the sweep is reduced, the flow changes from a classical vortex pattern at 75-deg sweep to that of a thin separation bubble with a shock above the bubble at 67.5-deg

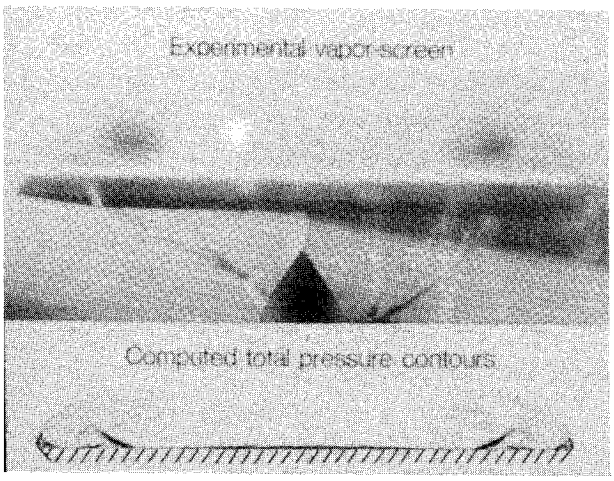

Fig. 7 Flowfield comparison, $M_\infty = 1.70$, $\alpha = 8$ deg, $\Lambda_{LE} = 75$ deg.

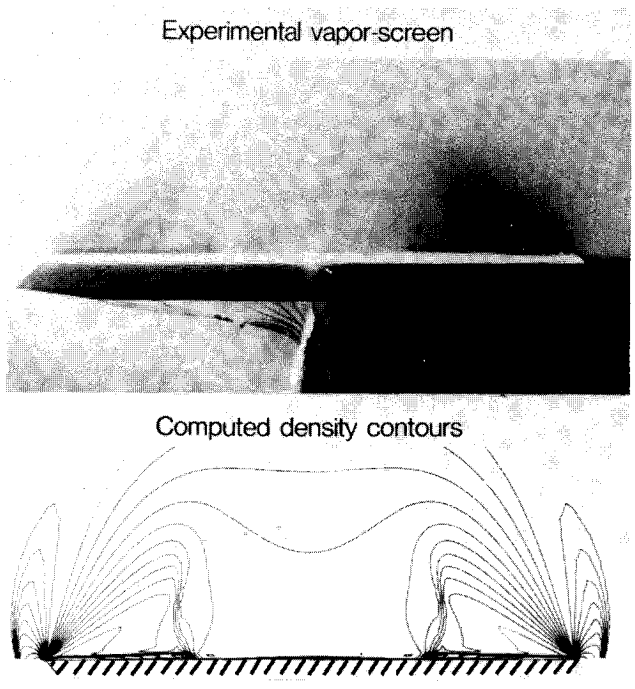

Fig. 8 Flowfield comparison, $M_\infty = 2.80$, $\alpha = 8$ deg, $\Lambda_{LE} = 67.5$ deg.

sweep. With further decrease in sweep angle, the bubble thins, and the shock position moves inboard. There is good agreement of the computed and measured pressures.

Computed flowfields at two of the above conditions are compared in Figs. 7 and 8 to vapor screen photographs from the experiment. The vapor screen photographs are taken from the rear and above the wind-tunnel model; the pressure tubing exits from the lower surface of the wing trailing edge and can be seen in the photograph.

The first condition corresponds to a classical vortex separation; vapor screen photographs from the experiment are compared with computed contours of total pressure in Fig. 7. The size and location of both the primary and secondary vortices coincide closely between theory and experiment.

The second comparison is at a higher Mach number and a lower sweep angle and corresponds experimentally to a thin bubble separation developing under an upper-surface shock. The vapor screen photograph is compared in Fig. 8 with computed density contours. The overall agreement of the computations with the experiment is quite good. Close examination of the computed results indicates a very thin separation bubble underneath the shock. These two comparisons illustrate that the total pressure contours serve to best define the vortical flow patterns on the wing, whereas the density contours serve to define more clearly the shock patterns over the wing. In the vortical flow regions, the density contours are more nearly circular than the total pressure contours, the latter in better agreement with the vapor screen information; above the viscous regions, the total pressure contours are in evidence only at a shock and do not show, for instance, an isentropic expansion or compression wave.

In order to assess the limitations of the conical Navier-Stokes approximation, several three-dimensional computations have been made for the 75-deg swept wing at a Mach number of 1.7, corresponding to separated leading-edge flow with both primary and secondary vortices. In order to resolve the apex region sufficiently, the solutions were obtained on a conical grid, extending from 5% of the root chord to the trailing edge. The grid in each of the crossflow planes corresponds to that used previously for the conical solutions; 20 planes were distributed uniformly in the axial direction so that 250,000 grid points defined the computational grid. Since the flow is supersonic, the inflow conditions were obtained from the conical assumption, and the outflow conditions were obtained by extrapolation. Solutions starting from freestream initialization were obtained in less than 2 hr on the VPS-32 computer at NASA Langley.

The spanwise pressure coefficient at several longitudinal positions is shown in Fig. 9 at angles of attack of 8 and 20 deg. In general, the streamwise variation in pressure is small, and the spanwise pressure distribution is quite similar to the previous conical results. The minimum pressure at each streamwise station decreases with distance away from the apex, which is consistent with the increase in Reynolds number with distance from the apex. The pressures at the higher angle of attack show somewhat less chordwise variation than the lower angle of attack; the flow at the higher angle of attack is dominated by the sharp-edged separation vortex and is less influenced by the secondary separation. Density contours indicate that the flow pattern is very similar at all stations along the root chord, evidencing the primary and secondary vortex patterns observed experimentally. At the higher angle of attack, the separated flow region is much

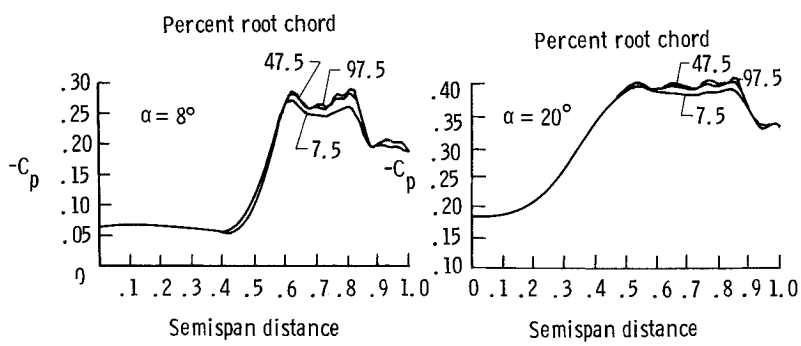

Fig. 9 Three-dimensional effects for sharp-edged delta wing, $M_\infty = 1.70$, $\Lambda_{LE} = 75$ deg.

larger, and a weak crossflow shock oriented parallel to the wing develops on the leeward side above the plane of symmetry. The plane of symmetry shock is also observed in the vapor screens of Ref. 2. Limiting streamlines on the upper surface also indicate that the flow is nearly conical over the entire length of the body. This is also consistent with the experimental oil flow patterns of Miller and Wood.[2] The present results differ from the results of Rizzetta and Shang[4] and Buter and Rizzetta,[5] which indicate the flow to be largely nonconical in the apex region. The differences are attributed to the lack of resolution in those results in the apex region, especially in the normal direction. The lack of resolution is apparent in the inviscid solutions of Ref. 4, which should be conical over the entire wing, but are decidedly not in the apex region.

It should be noted that the conical-flow equations also allow for streamwise variation through the definition of Reynolds number at the specified crossflow station. The resulting solution is, however, only locally valid. Unlike the three-dimensional equations, the conical equations do not properly account for the upstream influence of the flow and, instead, assume that the flow some infinitesimal distance upstream will be conically similar to the flow at the specified crossflow station. When the streamwise flow variation is small, as shown previously, the conical equations provide an excellent approximation to the full three-dimensional equations.

Concluding Remarks

Solutions to the Navier-Stokes equations for the flow over delta wings, with emphasis on the separated vortical flows developing on the lee side at high angles of attack, are obtained. The computations are made with a recently developed implicit algorithm, employing upwind differencing for the pressure and convection terms and central differencing for the shear stress and heat-transfer terms. Solutions to both the three-dimensional equations and the approximate conical-flow equations are compared parametrically with an extensive experimental data base at supersonic speeds. The data base includes variations in leading-edge sweep angle, angle of attack, and Mach number. The computations indicate that the conical-flow approximation provides results in close agreement with the three-dimensional equations, even to angles of attack as high as 20 deg. Good agreement with the experimentally measured pressures and vapor screen photographs is obtained for the matrix of conditions investigated. The method predicts the classical pattern of vortical flow over a delta wing, with primary and secondary vortices on the leeward wing surface at high angles of attack and subsonic values of the Mach number defined normal to the wing leading edge. In close agreement with the experiment, the method predicts the transition to other flow patterns as the leading-edge sweep angle and leading-edge-normal Mach number are varied.

In Ref. 2, Miller and Wood applied several currently available methods based on linear theories, including a correction for vortex-induced lift, to the delta wing flows measured experimentally. The present results represent a substantial improvement, especially in the prediction of surface pressure, to those methods. The computational rate is approximately 30 μs per grid point per iteration; hence, each conical-flow solution requires several minutes on the VPS-32 computer at NASA Langley. As the method for conical flows is fairly efficient, it could be considered as a design tool for the development of improved aerodynamics surfaces.

References

[1]Stanbrook, A. and Squire, L. C., "Possible Types of Flow at Swept Leading Edges," *Aeronautical Quarterly*, Vol. 15, 1964, pp. 72–82.

[2]Miller, D. S. and Wood, R. M., "Lee-Side Flow Over Delta Wings at Supersonic Speeds," NASA TP-2430, June 1985.

[3]Vigneron, Y. C., Rakich, J. V., and Tannehill, J. C., "Calculation of Supersonic Viscous Flow Over Delta Wings With Sharp Subsonic Leading Edges," AIAA Paper 78-1137, July 1978.

[4]Rizzetta, D. P. and Shang, J. S., "Numerical Simulation of Leading Edge Vortex Flows," *AIAA Journal*, Vol. 24, Feb. 1986, pp. 237–245.

[5]Buter, T. A. and Rizzetta, D. P., "Steady Supersonic Navier-Stokes Solutions of a 75 deg Delta Wing," *Proceedings of the Vortex Flow Aerodynamics Conference,* NASA Langley Research Center, Hampton, VA, NASA CP-2416, Oct. 1985.

[6]Fujii, K. and Kutler, P., "Numerical Simulation of the Leading Edge Separation Vortex for a Wing and Strake-Wing Configuration," AIAA Paper 83-1908, July 1983.

[7]Fujii, K. and Kutler, P., "Numerical Simulation of the Viscous Flow Over Three-Dimensional Complicated Geometries," AIAA Paper 84-1550, June 1984.

[8]McRae, D. S., "A Numerical Study of Supersonic Viscous Cone Flow at High Angle of Attack," AIAA Paper 76-97, Jan. 1976.

[9]McRae, D. S. and Hussaini, M. Y., "Numerical Simulation of Supersonic Cone Flow at High Angle of Attack," AGARD CP-247, Paper 23, Oct. 1978.

[10]Thomas, J. L., van Leer, B., and Walters, R. W., "Implicit Flux-Split Schemes for the Euler Equations," AIAA Paper 85-1680, July 1985.

[11]Thomas, J. L. and Walters, R. W., "Upwind Relaxation Algorithms for the Navier-Stokes Equations," *AIAA Journal,* Vol. 25, April 1987, pp. 527–534; also AIAA Paper 85-1501-CP, July 1985.

[12]Monnerie, B. and Werlé, H., "Etude de l'Ecoulement Supersonic et Hypersonique Autour d'une Aile Elancee en Incidence," AGARD CP-30, Paper No. 23, May 1968.

[13]Newsome, R. and Thomas, J. L., "Computation of Leading-Edge Vortex Flows," NASA Langley Research Center, Hampton, VA, NASA CP-2416, Oct. 1985.

[14]Murman, E. M., Powell, K. G., Miller, D. S., and Wood, R. M., "Comparison of Computations and Experimental Data for Leading Edge Vortices—Effects of Yaw and Vortex Flaps," AIAA Paper 86-0439, Jan. 1986.